J. Fluid Mech. (2007), *vol.* 585, *pp.* 73–92.
doi:10.1017/S0022112007006489 Printed in the United Kingdom

On the role of the Knudsen layer in rapid granular flows

J. E. GALVIN[1,3], C. M. HRENYA[1]† AND R. D. WILDMAN[2]

[1]Department of Chemical and Biological Engineering, University of Colorado, Boulder, CO 80309-0424, USA

[2]Wolfson School of Mechanical and Manufacturing Engineering, Loughborough University, Loughborough, Leicestershire, LE11 3TU, UK

[3]United States Department of Energy National Energy Technology Laboratory (NETL), Morgantown, WV 26507-0880, USA

(Received 11 September 2006 and in revised form 15 March 2007)

A combination of molecular dynamics simulations, theoretical predictions and previous experiments are used in a two-part study to determine the role of the Knudsen layer in rapid granular flows. First, a robust criterion for the identification of the thickness of the Knudsen layer is established: a rapid deterioration in Navier–Stokes order prediction of the heat flux is found to occur in the Knudsen layer. For (experimental) systems in which heat flux measurements are not easily obtained, a rule-of-thumb for estimating the Knudsen layer thickness follows, namely that such effects are evident within 2.5 (local) mean free paths of a given boundary. Secondly, comparisons of simulation and experimental data with Navier–Stokes order theory are used to provide a measure as to when Knudsen-layer effects become non-negligible. Specifically, predictions that do not account for the presence of a Knudsen layer appear reliable for Knudsen layers collectively composing up to 20 % of the domain, whereas deterioration of such predictions becomes apparent when the domain is fully comprised of the Knudsen layer.

1. Introduction

Many practical granular flows are characterized by a lack of separation of length and time scales. Correspondingly, the appropriateness of continuum descriptions based on such an assumption has been a topic of ongoing debate (see, for example, Kadanoff 1999; Goldhirsch 2003). The analogous molecular system is a rarefied gas, which is characterized by a relatively high value of the Knudsen number, defined as $Kn = \lambda/L_{grad}$, where λ is the mean free path and L_{grad} is the length scale characterizing spatial variations in the hydrodynamic variables (Chapman & Cowling 1970). Such systems, which lack a clear separation of scales, are characterized by large λ and/or small L_{grad}, e.g. dilute flows, flow through microchannels, high-Mach-number (Ma) flows, low-Reynolds-number (Re) flows (where $Kn \propto Ma/Re$ for molecular gases). Examples of granular flows with similar characteristics include shallow flows down an inclined plane (Forterre & Pouliquen 2001), supersonic flow past a wedge (Rericha *et al.* 2002), non-heaping grains at low gas pressure (Behringer *et al.* 2002), dilute flows past stationary objects (Wassgren *et al.* 2003) and the top layer of a vertically

† Author to whom correspondence should be addressed: hrenya@colorado.edu.

vibrated open system (Brey, Ruiz-Montero & Moreno 2001; Goldhirsch, Noskowicz & Bar-Lev 2004; Martin, Huntley & Wildman 2006).

In molecular systems, the appropriate mathematical description of a gas depends on the value of Kn, since constitutive relations are derived based on series expansions about small values of Kn (Chapman & Cowling 1970; Ferziger & Kaper 1972). Generally speaking, for $Kn < 10^{-2}$ (continuum regime), Navier–Stokes order hydrodynamics coupled with a no-slip boundary condition is appropriate. For $10^{-2} < Kn < 10^{-1}$ (slip regime), a slip (apparent) boundary condition is required to account for the presence of a non-negligible Knudsen layer (Rosner & Papadopoulos 1996). (Note that all wall-bounded flows contain a Knudsen layer adjacent to the wall in which the detailed nature of particle–wall collisions impacts transport as opposed to particle–particle collisions, which dictate behaviour in the bulk interior. Similarly, systems with a free surface also display a Knudsen layer. For example, in a vibrated vessel with an open top, particles at the top surface are more likely to follow a parabolic trajectory than to engage in particle–particle collisions. Regardless of whether the boundary is open or closed, however, if the Knudsen layer is small relative to the characteristic system size, then an approach which does not incorporate the effects of the Knudsen layer is appropriate over the entire domain.) At even higher Kn, namely $10^{-1} < Kn < 10$ (transition regime), higher-order terms in the Chapman–Enskog expansion (about Kn) are required, which increases the order of the governing equations and the corresponding boundary conditions. For example, the Burnett equations require second-order slip boundary conditions to account for the Knudsen layer. Higher-order boundary conditions cannot be obtained solely from physical principles, and such descriptions remain an active area of research. Furthermore, solutions at the Burnett level are inherently unstable. One proposed solution to these problems is to consider relaxation in the system as a method for providing stability and closure (Jin & Slemrod 2001). Despite this progress, however, for $Kn > 10$ (free molecular flow), a higher-order treatment for the domain interior coupled with a Knudsen layer at the boundary remains difficult to realize (Jin & Slemrod 2001).

In the context of granular flows, the vast majority of theoretical contributions have focused on the continuum regime (Navier–Stokes order hydrodynamics without modification to account for a Knudsen layer), whereas less attention has been focused on systems in which the separation of scales is not clear cut. At the high Kn limit (free molecular flows), Kumaran developed a model for shear flows with smooth particles (Kumaran 1997) and rough particle–wall interactions (Kumaran 2005), respectively. For transitional flows, Sela & Goldhirsch (1998) derived Burnett-order equations for dilute systems. Finally, several previous investigations have recognized the importance of the Knudsen layer at the open end of a vertically vibrated system (Brey *et al.* 2001; Goldhirsch *et al.* 2004; Martin *et al.* 2006). Specifically, Martin *et al.* (2006) provided two estimates for the thickness of the Kn layer and Brey *et al.* (2001) developed a boundary condition to account for the Knudsen-layer effects. Both works are specific to the free surface of the vertically vibrated system and do not consider the role of the Knudsen layer at the bottom (vibrating) boundary.

To build on the previous efforts, the aim of the current work is twofold: (i) to develop a robust method for determining the thickness of the Knudsen layer at a closed boundary; and (ii) to assess the appropriateness of a continuum-regime treatment (Navier–Stokes order theory, coupled with no-slip conditions) for systems with various Knudsen-layer widths (relative to system size). For (i), molecular dynamics (MD) simulations of a quiescent (no mean motion) system with an imposed temperature gradient are used. This effort draws on previous work for the analogous molecular-gas (elastic) system investigated by Mackowski, Papadopoulos & Rosner (1999) and Pan

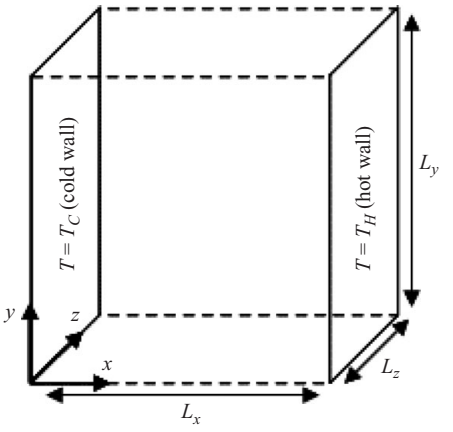

FIGURE 1. Schematic of the bounded conduction system.

et al. (2006). For (ii), a combination of MD simulations, (Navier–Stokes order) theory, and previous experiments are used. The results give rise to a general criterion for the identification of the Knudsen-layer thickness based on heat flux measurements, and demonstrate under what conditions a Navier–Stokes order treatment that does not incorporate the effects of a Knudsen layer begins to deteriorate.

2. Molecular dynamics (MD) simulations: computational algorithm

This work employs three-dimensional MD simulations of uniform particles to examine the effects of a Knudsen layer at the boundary. The particles are treated as inelastic, frictionless spheres. Particle collisions are assumed binary and instantaneous (i.e. hard-sphere assumption). The three-dimensional simulation domain is bounded on the left- and right-hand sides by motionless walls of constant, but not necessarily equal, granular temperature (figure 1). The remaining four walls (top, bottom, front and back) are periodic. No body forces are present, and thus the system is characterized by zero mean flow. The simulation discussed herein has been described elsewhere; for additional details, see Dahl & Hrenya (2004) and Galvin, Dahl & Hrenya (2005).

As mentioned above, the simulation is bounded on the left- and right-hand sides by walls of a set temperature (T_{set}). The boundary conditions are determined using a method for thermal walls presented by Cercignani (1987) and Pöschel and Schwager (2005), and are slightly different from those of Dahl & Hrenya (2004) and Galvin *et al.* (2005). Particles colliding with one of the bounding walls are given a post-collisional velocity that is consistent with the T_{set} of the wall with which they collided. Specifically, the post-collisional components of particle velocity (c_{post}) that are parallel to the wall (i.e. in the y- and z-directions) are determined using the Box–Muller method for generating two tangential Gaussian distributions (Press *et al.* 1992):

$$c_{post,y} = \sqrt{-\frac{2T_{set}}{m_i}\ln(z_1)}\,\cos(2\pi z_2), \tag{1}$$

$$c_{post,z} = \sqrt{-\frac{2T_{set}}{m_i}\ln(z_3)}\,\sin(2\pi z_4), \tag{2}$$

where $z_1 - z_4$ are random numbers uniformly distributed in the interval [0, 1]. The post-collisional component of particle velocity normal to the wall (in the x-direction)

is given by

$$c_{post,x} = \sqrt{-\frac{2T_{set}}{m_i}\ln(z_5)}, \tag{3}$$

where z_5 is a random number again uniformly distributed in the interval [0, 1]. The sign (+ or −) of the pre-collisional component of particle velocity normal to the wall is reversed after collision. The four remaining boundaries are standard periodic boundaries such that a particle crossing through one of these boundaries is returned through the opposing boundary with the same velocity and relative position.

The particles in the simulation are initially loaded onto a cubic lattice. The particles are then moved from their node positions by a small random displacement and any initial overlaps are resolved by making further random displacements in their position. As an estimate, the initial particle velocities are taken from a Maxwellian distribution that is consistent with their position along an assumed linear temperature gradient between the two set temperature walls. The actual temperature profile that develops between the two set temperature walls is nonlinear, but the linear profile provides a basis for an initial condition.

The simulation proceeds in time via a hard-particle/overlap algorithm (Hopkins & Louge 1991). In this method, the simulation progresses by making a series of small time steps during which the particles are moved along their linear trajectories. After each time step, any collisions are detected by searching for overlaps between particles or between a particle and a wall. Collisions are resolved using a hard-sphere model. For further details on the particle advancement algorithm, see Dahl & Hrenya (2004).

The input parameters for each simulation include L_x, L_y and L_z, the length of the simulation domain in the x-, y- and z-directions; d, the particle diameter; m, the mass of a particle; $\bar{\nu}$, the average solids volume fraction in the (entire) system; e, the coefficient of restitution; and T_C and T_H, the set values of wall temperature located at $x/L_x = 0$ and $x/L_x = 1$, respectively. The dimensionless parameters that characterize the system are $\bar{\nu}$, e, T_H/T_C, L_x/d, L_y/L_x and L_z/L_x. Here, $L_x/d = 35$ was selected to ensure that each simulation was described by $1/Kn > 5$, where the 'global' Knudsen number is defined as $Kn = \bar{\lambda}/L_x$ and $\bar{\lambda} = d/(6\bar{\nu})$ is the spatially averaged mean free path. Consequently, a given simulation will have a total number of particles (N) ranging from 4000 to 12000 depending on the values of the other dimensionless quantities ($\bar{\nu}$, L_y/L_x, L_z/L_x). In nearly all simulations, the periodic domain lengths are set equal ($L_y = L_z$). For $L_x/d = 35$, a value of $L_y/L_x = L_z/L_x = 1$ is used to ensure that the collected data are not sensitive to further increases in the periodic domain length. As a result, the simulation domain is cubic ($L_x = L_y = L_z$) and the characteristic dimension is hereinafter referred to as L. The remaining parameter space under investigation includes the temperature ratio (T_H/T_C) with set values of 1, 2 and 15, $\bar{\nu} = 0.025$–0.15 ($Kn = 1.9 \times 10^{-1} - 3.2 \times 10^{-2}$) and $e = 0.8 - 1$. For convenience, the dimensional quantities m and L_x are set equal to 1.

The outputs from the simulation include lateral profiles of the solids volume fraction (ν), granular temperature (T) and heat flux ($\boldsymbol{q}$), where the granular temperature is defined as $T = 1/3\langle C^2\rangle$ and $\boldsymbol{C}$ is the fluctuating velocity. Note that the dissipation rate (γ) is also collected in order to check whether the energy balance for the simulation is satisfied ($\nabla \cdot \boldsymbol{q} = -\gamma$; see (17)), which serves as a verification of the simulation results. The check indicates that the energy balance is indeed satisfied; further details on calculating this quantity and the corresponding verification can be found in Hrenya, Galvin & Wildman (2007).

Data collection begins once 10 000–20 000 collisions per particle have occurred (depending on $\bar{\nu}$). To ensure that a statistical steady state has been achieved, the x-coordinate of the centre-of-mass location of the particles and the granular temperature are monitored during the data collection period to make sure they change no more than 5 % during the data collection interval (See Dahl & Hrenya 2004 for further details).

Several output quantities (T, $\boldsymbol{q}$, γ) are a function of the fluctuating velocity ($\boldsymbol{C}$), which in turn is defined relative to a local mass-average velocity. In this effort, a zero mass-average velocity is assumed in all calculations for the sake of computational efficiency. This assumption does not impact the results, as was established by Galvin, Dahl & Hrenya (2005). Accordingly, the fluctuating particle velocity is equal to the instantaneous particle velocity ($\boldsymbol{c}$) and the two may be used interchangeably.

The spatial variation of the output quantities is determined by dividing the domain into thin rectangular boxes aligned in the direction parallel to the set-temperature walls. The width of each data collection strip (Δx) is set slightly wider than the particle diameter. Therefore, the current simulations include 30 data collection strips. The width of the collection strip (i.e. number of collection strips) was set so that the collected data do not change meaningfully with further resolution in the collection width (i.e. increased number of collection strips).

As mentioned earlier, two types of data are reported in the simulation: hydrodynamic variables (ν, T) and constitutive quantities ($\boldsymbol{q}$). The solids volume fraction within each data collection strip is found by including only the volume of the particles that are within the data collection strip. The granular temperature within each data collection strip is found by including only the granular temperature of particles whose centres reside within the data collection strip at the instant of measurement (see Dahl & Hrenya 2004 for further details).

The total heat flux ($\boldsymbol{q}$) consists of a kinetic component ($\boldsymbol{q}_k$) and a collisional component ($\boldsymbol{q}_c$). The heat flux is calculated following the methods used by Herbst, Müller & Zippelius (2005) in which the kinetic contribution of the heat flux is determined using

$$q_{k,a,strip} = \frac{1}{V_{strip}} \sum_{i=1}^{n_{strip}} \frac{1}{2} m C_{strip}^2 C_{a,strip}. \tag{4}$$

In this equation, $C_{a,strip}$ is the fluctuating particle velocity in that strip in the a direction (where a can be x, y or z), $C_{strip}^2 = \boldsymbol{C}_{strip} \cdot \boldsymbol{C}_{strip}$, V_{strip} is the volume of the strip ($V_{strip} = L_z L_y \Delta x$) and n_{strip} is the number of particles whose centres reside within the data collection strip. The collisional component of the heat flux is found by

$$q_{c,a,strip} = \frac{1}{2V_{strip}\Delta t} \sum_{coll_{strip}} \left(\Delta E_1 - \Delta E_2\right) D k_a, \tag{5}$$

where Δt is the elapsed time since data collection was initiated, D is the distance between the particle centres, k_a is the a component of the unit vector pointing from the centre of particle 1 toward the centre of particle 2 ($a = x$, y, or z), ΔE_1 is the change in energy of particle 1 owing to a collision with particle 2 and ΔE_2 is the change in energy of particle 2 owing to a collision with particle 1. For a given particle, ΔE is defined as

$$\Delta E = \tfrac{1}{2} m \left(C_{post}^2 - C_{pre}^2\right), \tag{6}$$

where the mass and fluctuation velocity are those quantities associated with the given particle. Note that collisional heat flux (equation (5)) is found by summing only the heat flux of particles whose centres reside within the data collection strip during the collision (summation over $coll_{strip}$). In the event that the centres of the two colliding particles lie in different strips, the collisional heat flux is divided equally between the adjacent data collection strips in which the particle centres reside.

Unless otherwise noted, the data collection phase of each simulation comprises 50 000 collisions per particle during which 1 000 000 evenly spaced instantaneous measurements of solids volume fraction, granular temperature and the kinetic components of the heat flux are made. The collisional components of the heat flux are evaluated as a summation over all collisions in the system during the data collection portion of the simulation. At the end of the simulation, the average of these measurements is calculated and reported. Measurements corresponding to the strips adjacent to the bounding walls are not reported since such measurements inherently include volume exclusion effects caused by the solid boundary (a particle cannot penetrate a solid boundary). For example, as the strip width next to the boundary approaches zero, the volume fraction at that strip will also approach zero. Such a width-sensitive measurement is not reflective of the actual hydrodynamic value, and is instead an inherent artefact of the averaging technique. Note that if the strip width is at least one particle diameter, which is the case for all systems examined here, such volume exclusion effects will only impact the strip adjacent to the boundary. Hence, the values obtained at strips adjacent to the boundaries are not being reported here. It is worth noting that because this wall value is not reported, the average solids volume fraction obtained by integrating the reported solids volume profile will not appear to be in perfect agreement with the average solids fraction initially set in the simulation, but the difference is small and the reported measurements are indeed accurate. It is also worth noting that the observed temperature ratio will not match the set value of the temperature ratio (unless the ratio equals unity). The reason for the apparent mismatch can be traced to the thermal wall boundary condition, which specifies the temperature of only the outgoing particles (those which have collided with the wall) but says nothing about incoming particles (which will have a lower temperature). Since the measured temperature in the strip adjacent to the wall includes both types of particle (incoming and outgoing), the observed temperature will be lower than the set temperature. For simplicity, only the characteristic volume fraction and temperature ratio initially set in the simulation are reported.

3. Theoretical predictions

To help elucidate the degree and impact of Knudsen-layer effects, both constitutive quantities (q_x) and hydrodynamic variables (ν and T) obtained from MD simulations are compared to predictions obtained from two continuum theories for rapid granular flows. In particular, the kinetic-theory-based predictions of Jenkins (1998) and Garzó & Dufty (1999) are considered. These theories are both targeted at uniform inelastic frictionless spheres engaging in instantaneous binary collisions. Hence, the assumptions inherent in both theories mimic those of the MD simulations. Furthermore, both theories are of Navier–Stokes order (i.e. the constitutive relations are up to first order in spatial gradients). A key difference between the two approaches lies in the derivation process; the theory of Jenkins (1998) is based on an expansion about an elastic base case, while the theory of Garzó & Dufty (1999) is based on

an expansion about a homogeneous cooling state. Correspondingly, the resulting constitutive relations take on a different form, the specifics of which are given below.

It is important to note that two distinct methods are used to compare the MD simulation data to the theoretical predictions. Specifically, the theoretical predictions for the constitutive quantity of interest (q_x) are obtained using MD simulation profiles as inputs to the theory, whereas the theoretical predictions for the hydrodynamic variables (ν and T) are obtained by solving the appropriate boundary-value problem (BVP). The type of information gleaned from each type of comparison is different in character, as is detailed in the following two sections.

3.1. *Heat flux: using MD data as inputs to theory*

According to the two theories being considered here, the expressions for the heat flux for the bounded conduction problem are:

Jenkins (1998)

$$q_x = -\left\{\frac{75}{64}\frac{m}{d^2\sqrt{\pi}}\sqrt{T}\left[\frac{1}{g_0}+\frac{24}{5}\nu+\frac{144}{25}\left(1+\frac{32}{9\pi}\right)\nu^2 g_0\right]\right\}\frac{\mathrm{d}T}{\mathrm{d}x}, \tag{7}$$

Garzó & Dufty (1999)

$$q_x = -\left\{\frac{75}{64}\frac{m}{d^2\sqrt{\pi}}\sqrt{T}\left[k_k^*\left(1+\tfrac{6}{5}\nu g_0(1+e)\right)+\frac{256\nu^2}{25\pi}g_0(1+e)\left(1+\tfrac{7}{32}c^*\right)\right]\right\}\frac{\mathrm{d}T}{\mathrm{d}x}$$
$$-\left\{\frac{25}{128}\frac{md\sqrt{\pi}T^{3/2}}{\nu}\left[\mu_k^*\left(1+\frac{6\nu}{5}g_0(1+e)\right)\right]\right\}\frac{\mathrm{d}n}{\mathrm{d}x}, \tag{8}$$

where

$$k_k^* = \tfrac{2}{3}\left(\nu_k^*-2\varsigma^{(0)*}\right)^{-1}\left[1+\tfrac{1}{2}(1+p^*)c^*+\frac{6\nu}{10}g_0(1+e)^2\right.$$
$$\left.\times\left\{2e-1+\left(\tfrac{1}{2}(1+e)-\frac{5}{3(1+e)}\right)c^*\right\}\right], \tag{9}$$

$$\nu_k^* = \tfrac{1}{3}(1+e)g_0\left[1+\tfrac{33}{16}(1-e)+\frac{19-3e}{1024}c^*\right], \tag{10}$$

$$\varsigma^{(0)*} = \tfrac{5}{12}g_0(1-e^2)\left(1+\tfrac{3}{32}c^*\right), \tag{11}$$

$$p^* = 1+2\nu(1+e)g_0, \tag{12}$$

$$c^* = 32(1-e)(1-2e^2)[81-17e+30e^2(1-e)]^{-1}, \tag{13}$$

$$\mu_k^* = 2\left(2\nu_k^*-3\varsigma^{(0)*}\right)^{-1}\left\{\left(1+n\frac{\partial\ln g_0}{\partial n}\right)\varsigma^{(0)*}k_k^*+\frac{p^*}{3}\left(1+n\frac{\partial\ln p^*}{\partial n}\right)c^*\right.$$
$$\left.-\frac{12\nu}{15}g_0\left(1+\frac{1}{2}n\frac{\partial\ln g_0}{\partial n}\right)(1+e)\left[e(1-e)+\tfrac{1}{4}\left(\tfrac{4}{3}+e(1-e)\right)c^*\right]\right\}, \tag{14}$$

where m refers to the particle mass, d is the particle diameter, e is the restitution coefficient, $n=6\nu/(\pi d^3)$ is the particle number density, and g_0 is the radial distribution function at contact, described here using the Carnahan & Starling (1969) expression:

$$g_0 = \frac{2-\nu}{2(1-\nu)^3}. \tag{15}$$

The constitutive relations for the heat flux are seen to depend on both constant material properties (d and m for both theories, as well as e for the Garzó & Dufty

(1999) theory) and hydrodynamic variables (ν and T). For the purposes of this work, it is important to note that the MD profiles for the hydrodynamic variables (ν and T) are used as inputs to the theoretical expressions for q_x (rather than the ν and T profiles obtained from the solution of the BVP, as described below). In this manner, any errors arising in the prediction of ν and T are not propagated to the q_x prediction, which thereby makes the comparison between the theoretical predictions for q_x (equations (7) and (8)) and those extracted directly from MD (equations (4) and (5)) more clear-cut.

3.2. *Concentration and temperature: solution of boundary-value problem (BVP)*

In addition to the heat flux comparison outlined above, comparisons between theory and MD simulations are also made for the hydrodynamic variables ν and T. Unlike the previous comparison, however, these profiles are determined via solution of the boundary-value problem describing the system. In this steady-state fully developed and quiescent flow, the conservation of mass is identically satisfied, and the conservation of momentum and the balance of granular energy take the following forms, respectively:

$$\frac{\mathrm{d}P}{\mathrm{d}x} = 0 \quad (\text{thus } P = \text{constant}) \tag{16}$$

and

$$\frac{\mathrm{d}q_x}{\mathrm{d}x} = -\gamma, \tag{17}$$

where P is the pressure and γ is the dissipation rate of granular energy per unit volume. The constitutive relations for q_x are given by (7) and (8) for the two theories, and the corresponding pressures and dissipation rates for the system considered herein are given by:

Jenkins (1998)

$$P = \frac{6\nu}{\pi d^3} mT[1 + 4\nu g_0], \tag{18}$$

$$\gamma = \frac{24\nu g_0}{d\sqrt{\pi}}(1 - e)mnT^{3/2}, \tag{19}$$

Garzó & Dufty (1999)

$$P = \frac{6\nu}{\pi d^3} mT[1 + 2\nu(1 + e)g_0], \tag{20}$$

$$\gamma = \frac{12\nu g_0}{d\sqrt{\pi}}(1 - e^2)\left(1 + \tfrac{3}{32}c^*\right)mnT^{3/2}. \tag{21}$$

The number of particles is set via an auxiliary integral equation for the average packing fraction (Arnarson & Jenkins 2004; Wildman *et al.* 2006):

$$\bar{\nu} = \frac{1}{L_x}\int_0^{L_x} \nu \,\mathrm{d}x \tag{22}$$

which, to aid solution, is expressed as a differential equation

$$\frac{\mathrm{d}\overline{\nu_{cum}}}{\mathrm{d}x} = \frac{1}{L_x}\nu(x), \tag{23}$$

where the subscript *cum* indicates that it refers to the cumulative determination of average packing fraction (i.e. it is a function of x) as opposed to the overall packing fraction of the system, $\bar{\nu}$.

To solve for the four unknowns $\overline{\nu_{cum}}$, ν, T and q_x, the four first-order ordinary differential equations ((7) or (8), (16), (17) and (23)) require boundary conditions for

the granular temperature and the average packing fraction:

$$T(x = 0) = T_C, \tag{24}$$

$$T(x = L_x) = T_H, \tag{25}$$

$$\overline{\nu_{cum}}(x = 0) = 0, \tag{26}$$

and

$$\overline{\nu_{cum}}(x = L_x) = \frac{\pi d^3 N}{6V}. \tag{27}$$

where $V = L_x L_y L_z$ is the system volume. The resulting system of equations is solved using the Matlab bvp4c boundary-value solver (Kierzenka & Shampine 2001) with the numerical inputs described in § 2.

Recall that in the MD simulations, measurements corresponding to the strips adjacent to the bounding walls are disregarded. As a result, the MD system domain is effectively reduced and the parameters that characterize the resultant system (average volume fraction, temperature ratio of walls, etc.) are slightly different from the original input parameters. The characteristic domain length (L_x) for the reduced system is calculated based on the original domain length minus the width of three collection strips (one strip width arising from each bounding wall and an additional strip width since measurements are reported at the midpoint of a strip). Hence, the values of L_x/d, L_y/L_x and L_z/L_x, are all adjusted. The characteristic temperature ratio (T_H/T_C) is calculated based on the temperatures measured in the strips immediately next to those adjacent to the bounding walls. The average solids volume fraction is adjusted based on the solids volume that is actually present in the reduced domain. The adjusted values are then used to define the boundary-value problem in order to obtain a one-to-one comparison between the reported MD system and the boundary-value problem.

As will be demonstrated below, the heat flux comparison described in the previous section helps to pinpoint the boundary between the Knudsen layer and the bulk interior, while the solution of the BVP serves as an indicator of the appropriateness of Navier–Stokes order theory, coupled with no-slip conditions, for systems with Knudsen layers of various thicknesses (relative to the system size).

4. Results and discussion

As detailed above, the MD simulations were performed over a substantial parameter space. For brevity, the results presented herein are kept to a minimum and are representative of the complete set examined.

Before considering inelastic systems, it is helpful to look at the more familiar case of a hard-sphere molecular gas ($e = 1$). Figures 2(a) and 2(b) display the MD results for the solids fraction and temperature profiles, respectively, for a case in which $\bar{\nu} = 0.05$ and $T_H/T_C = 2$. As is consistent with the equation of state (equations (18) or (20)), the ν and T profiles are inversely related. The characteristic 'jump' in temperature at the wall, which is a hallmark of rarefied gases in the slip regime, is difficult to detect not only because of the scale of figure 2(b), but also because the value in the collection strip adjacent to the wall is not reported. Its presence, however, becomes apparent on a plot of the corresponding first derivative of temperature, as is shown in figure 2(c). First, the $\mathrm{d}T/\mathrm{d}x$ behaviour in the interior of the domain is distinct from that near the walls: an abrupt increase in the magnitude of $\mathrm{d}T/\mathrm{d}x$ is observed near both walls, which is consistent with the presence of a temperature jump.

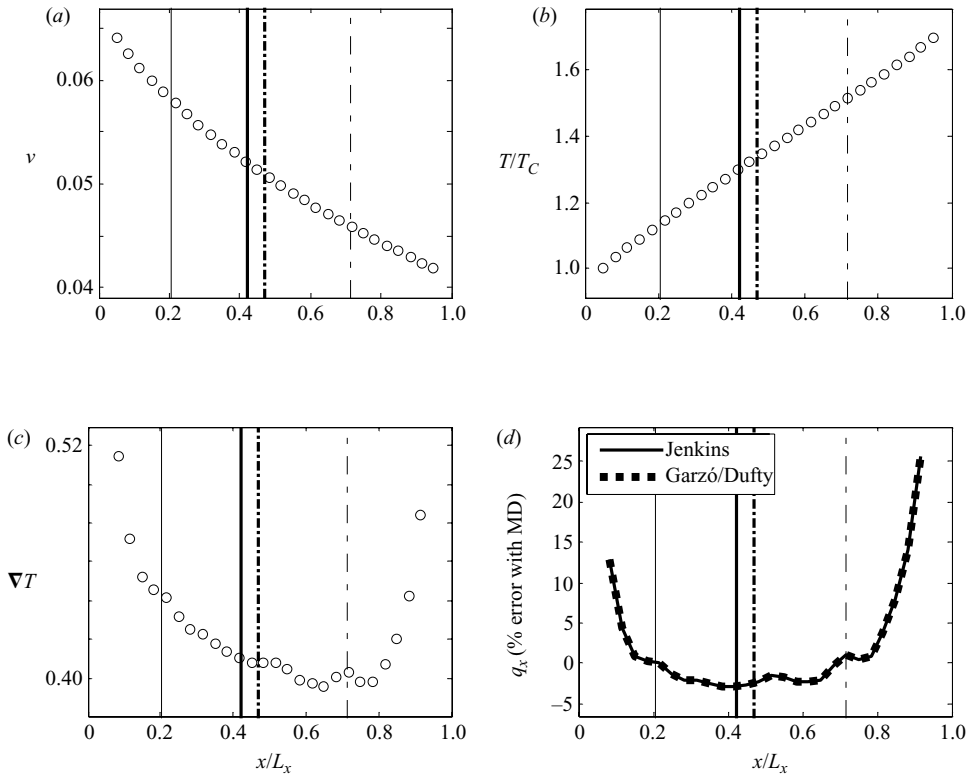

FIGURE 2. MD profiles of (*a*) solids volume fraction, (*b*) non-dimensional granular temperature and (*c*) the first derivative in granular temperature, (*d*) the percentage error in heat flux between MD simulations and theoretical predictions. MD simulations (circles); Jenkins (1998) predictions (thin solid line); Garzó & Dufty (1999) predictions (thick dotted line). Reciprocal local Knudsen numbers evaluated from the cold, left-hand (solid) and hot, right-hand (dash-dot) wall of 2.5 (thin) and 5.0 (thick) are indicated by the vertical lines. Relevant parameters are $e = 1$, $\bar{\nu} = 0.05$ $(1/Kn = 10.5)$, $T_H/T_C = 2$, $L/d = 35$. Data collection for this simulation involves 2 000 000 measurements over 100 000 collisions/particle.

Secondly, note that $\mathrm{d}T/\mathrm{d}x$ displays a local minimum in the interior of the domain (at $x/L_x = 0.75$). As pointed out by Pan *et al.* (2006), this behaviour is at odds with Fourier's law $q_x = -k(\mathrm{d}T/\mathrm{d}x)$ for heat conduction. More specifically, according to the energy balance for elastic systems ($e = 1$), the heat flux takes on a constant value (i.e. $q_x = -k(\mathrm{d}T/\mathrm{d}x) = \text{constant}$). Furthermore, both experiments and theory show that $k > 0$ and $\mathrm{d}k/\mathrm{d}T > 0$, i.e. k is a positive value that increases with temperature (Chapman & Cowling 1970; Bird 1994; Cercignani, Illner & Pulvirenti 1994; Sone 2002). Thus, as T increases, k also increases, and thus according to Fourier's law, $\mathrm{d}T/\mathrm{d}x$ must decrease to maintain q_x at a constant value. In contrast to this Fourier-law-based expectation, however, it is observed that while T, and thus k, increases as the hot wall is approached (from left to right in figure 2*b*), $\mathrm{d}T/\mathrm{d}x$ shows a remarkable increase for $x/L_x > 0.75$ (figure 2*c*). This violation of Fourier's law indicates that the Navier–Stokes order constitutive relation for heat flux is no longer appropriate near the hot wall, thereby indicating that Knudsen effects are playing a role.

The characteristics noted above, namely the abrupt shift in $\mathrm{d}T/\mathrm{d}x$ and the violation of Fourier's law, are tell-tale signs of the Knudsen layer in molecular gases. As

described below, however, such techniques for identifying the Knudsen layer prove less useful for inelastic systems. Hence, another criterion is introduced here which is found to work well in both elastic and inelastic systems. Specifically, the presence of a Knudsen layer near both boundaries is apparent when comparing the heat flux obtained from MD simulations to that obtained from (Navier–Stokes order) theory. This comparison is given in figure 2(*d*) using models based on the analysis of both Jenkins (1998) and Garzó & Dufty (1999). As described in § 3.1, the theoretical predictions for q_x are obtained using the MD profiles of ν and T as inputs to the theory, so mismatches cannot be traced to any potential errors in ν and T. Recall for this system ($e = 1$) that the heat flux should be constant, which is indeed what is obtained from the MD simulations (figure not shown). The resulting error in q_x between MD simulations and both theories (figure 2*d*) is only a few per cent in the interior of the domain, whereas it quickly increases to $\sim 10\,\%$ error and beyond toward the boundaries. As previous studies for molecular gases have shown that deviations from Fourier's law are small even in the presence of large thermal gradients (Ciccotti & Tenebaum 1980; Mareschal *et al.* 1987; Clause & Mareschal 1988; Santos & Garzó 1995), this abrupt mismatch can be traced to the presence of a Knudsen layer (as opposed to the presence of large gradients or, equivalently, large Kn). Furthermore, it is worth noting that Burnett order corrections to a dilute (Chapman & Cowling 1970) or dense (Goldhirsch, personal communication 2006) molecular gas make no contribution to the heat flux for a zero-mean-flow system, so errors are attributable to effects of at least super-Burnett order. Hence, these results are consistent with the findings of Pan *et al.* (2006), whose empirical fit of the Knudsen-layer heat flux obtained from direct-simulation Monte Carlo (DSMC) of a molecular gas is third-order in temperature derivatives, implying that the Knudsen effects are beyond Burnett order corrections.

Although the abrupt changes in the profiles of $\mathrm{d}T/\mathrm{d}x$ and the error in q_x predictions provide a clear demarcation between the Knudsen layer and bulk interior, such profiles are difficult to obtain experimentally (whereas extraction from MD simulations is straightforward). Hence, an alternative measure of the Knudsen-layer thickness based on the volume fraction profile is also proposed. The vertical lines in figure 2 provide such a measure. Specifically, these lines represent a reciprocal (local) Knudsen number, defined as:

$$\frac{1}{Kn_{wall}} = \frac{\ell_{wall}}{\lambda_{wall}} = \left(\frac{\ell}{\lambda}\right)_{wall},$$

where ℓ_{wall} is the distance between a given wall and a point interior to the domain (e.g. the vertical line) and λ_{wall} is the mean free path defined in terms of the average solids fraction ($\bar{\nu}_{wall}$) between the wall and the distance ℓ_{wall}. For three-dimensional systems, such as those considered here, $\lambda_{wall} = d/(6\bar{\nu}_{wall})$. In figure 2, values of $(\ell/\lambda)_{wall} = 2.5$ and 5 are represented by the thin lines and thick lines, respectively. Moreover, the solid lines represent $(\ell/\lambda)_{wall}$ values associated with the cold wall (left-hand boundary), whereas the dashed lines are those associated with the hot wall (right-hand boundary). As shown in figures 2(*c*) and 2(*d*), a value of $(\ell/\lambda)_{wall} = 2.5$ provides a good demarcation between the Knudsen layer and the interior of the flow since this marker coincides with the abrupt changes observed in the $\mathrm{d}T/\mathrm{d}x$ profile (figure 2*c*) and the rapid deterioration of Fourier's law (figure 2*d*).

The physical reasoning for the suggested Knudsen-layer cutoff of $(\ell/\lambda)_{wall} = 2.5$ is possible via a consideration of what is occurring at the molecular level. For the separation-of-scales assumption to hold in the interior of the domain (bulk region), the probability that a particle travels from the boundary to the domain interior without

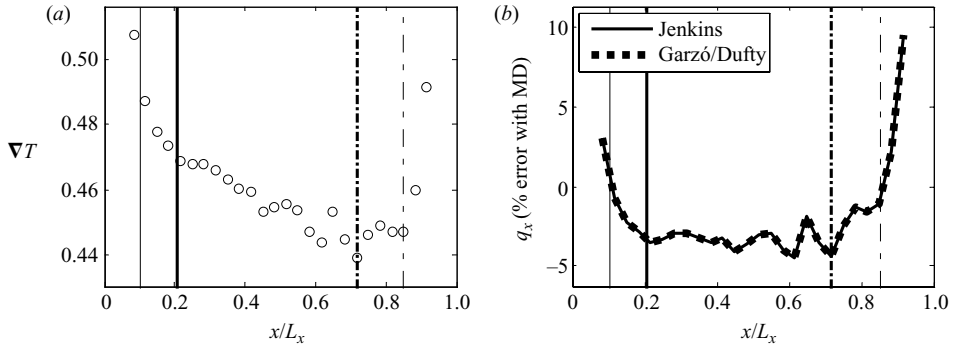

FIGURE 3. (*a*) MD profiles of solids volume fraction. (*b*) The percentage error in heat flux between MD simulations and theoretical predictions. Symbols and lines are as in figure 2. Relevant parameters are $e = 1$, $\bar{\nu} = 0.1$ ($1/Kn = 21.0$), $T_H/T_C = 2$, $L/d = 35$. Data collection for this simulation involves 2 000 000 measurements over 100 000 collisions/particle.

engaging in a collision must be small. For the simplified case of a homogeneous system (i.e. a molecular gas in thermal equilibrium), the probability (P) that a molecule of any speed travels a distance L_D without a collision occurring is approximated by (Chapman & Cowling 1970)

$$P = \exp(-1.04 L_D/\lambda),$$

where λ is the mean free path of the molecule. Note that for a value of $L_D/\lambda = 2.5$, the chance of a particle travelling a distance L_D without engaging in a collision is about 7 %. Thus, according to the demarcation proposed above, the bulk region 'begins' at a distance from the wall at which roughly 90 % of particles, having encountered the wall, have subsequently engaged in a collision. Correspondingly, the Knudsen-layer thickness (ℓ_{bl}), is proportional to the mean free path, or more specifically, $\ell_{bl} = 2.5\lambda_{wall}$. Hence, a smaller mean free path (denser system) results in a thinner Knudsen layer, which is consistent with others (Mackowski *et al.* 1999; Pan *et al.* 2006) who have noted that the Knudsen-layer thickness is proportional to the global Knudsen number ($Kn = \bar{\lambda}/L$).

To illustrate the robustness of the proposed Knudsen-layer criterion for elastic systems, figures 3 and 4 portray profiles analogous to those in figure 2, but for a different set of parameters. Specifically, figure 3 displays results for an increased average concentration of $\bar{\nu} = 0.10$, while figure 4 contains results for an increased temperature gradient, namely $T_H/T_C = 14$, also for $\bar{\nu} = 0.10$. For both cases, $(\ell/\lambda)_{wall} = 2.5$ is again seen to provide a good indicator of a sudden change in the $\mathrm{d}T/\mathrm{d}x$ profile (figures 3*a* and 4*a*) as well as the error associated with Fourier's law (figures 3*b* and 4*b*). The high-temperature-gradient case is particularly noteworthy, as the thicknesses of the two Knudsen layers are quite different from one another owing to the large difference in concentrations (and hence mean free paths) at each boundary.

The ability to identify the Knudsen layer for inelastic systems using $(\ell/\lambda)_{wall} = 2.5$ is demonstrated in figures 5 and 6, which contains profiles for a system analogous to those of figure 2 ($\bar{\nu} = 0.05$ and $T_H/T_C = 2$) and figure 4 ($\bar{\nu} = 0.10$ and $T_H/T_C = 14$), respectively, except that $e = 0.99$. Since dissipation is now present, the energy balance is no longer represented by $\nabla \cdot \boldsymbol{q} = 0$ ($q_x = \text{constant}$). Correspondingly, the test for the validity of Fourier's law, namely that $\mathrm{d}T/\mathrm{d}x$ should not take on a local minimum, is no longer valid. Despite the absence of such a test, the other salient features associated

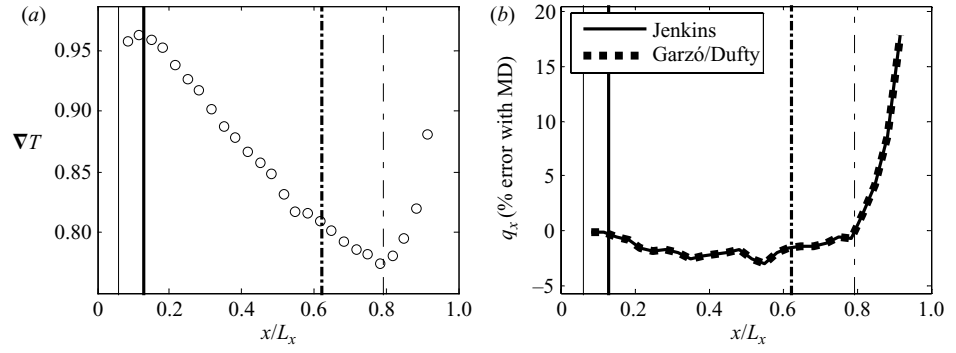

FIGURE 4. (*a*) MD profiles of solids volume fraction. (*b*) The percentage error in heat flux between MD simulations and theoretical predictions. Symbols and lines are as in figure 2. Relevant parameters are $e = 1$, $\bar{\nu} = 0.1$ $(1/Kn = 21.0)$, $T_H/T_C = 14$, $L/d = 35$.

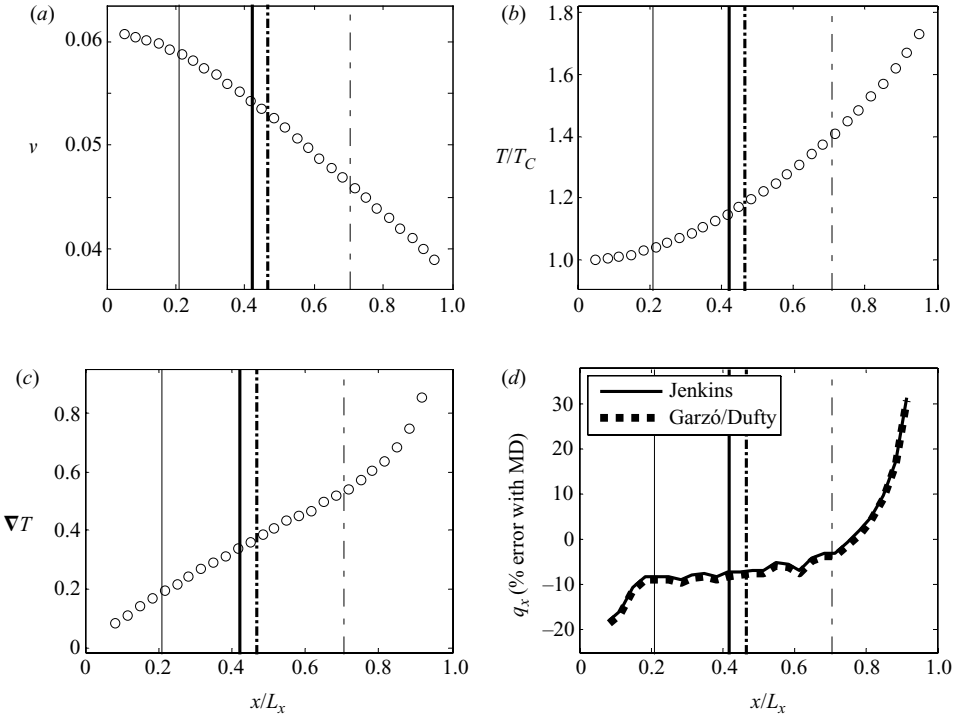

FIGURE 5. MD profiles of (*a*) solids volume fraction, (*b*) non-dimensional granular temperature and (*c*) the first derivative in granular temperature. (*d*) The percentage error in heat flux between MD simulations and theoretical predictions. Symbols and lines are as in figure 2. Relevant parameters: $e = 0.99$, $\bar{\nu} = 0.05$ $(1/Kn = 10.5)$, $T_H/T_C = 2$, $L/d = 35$.

with the Knudsen layer are present, namely the temperature jump as indicated by the distinct change in the temperature gradient $(\mathrm{d}T/\mathrm{d}x)$ profiles (figures 5*c* and 6*a*), and the pronounced deterioration of the heat flux predictions in the Knudsen layer (figures 5*d* and 6*b*), where it should be noted that the theories have incorporated the effect of inelasticity. Similar features are also exhibited in figure 7, in which $\bar{\nu} = 0.05$, $e = 0.9$ and $T_H/T_C = 1$. It is also worth noting that the theoretical prediction for q_x

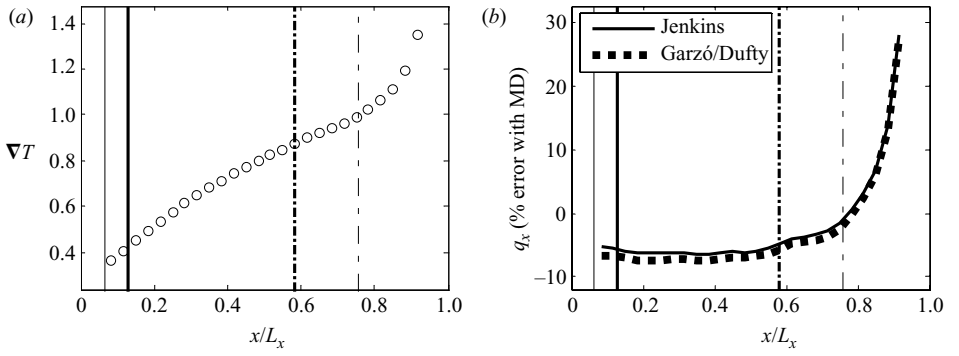

FIGURE 6. (*a*) MD profiles of solids volume fraction. (*b*) The percentage error in heat flux between MD simulations and theoretical predictions. Symbols and lines are as in figure 2. Relevant parameters are $e = 0.99$, $\bar{\nu} = 0.1$ $(1/Kn = 21.0)$, $T_H/T_C = 14$, $L/d = 35$.

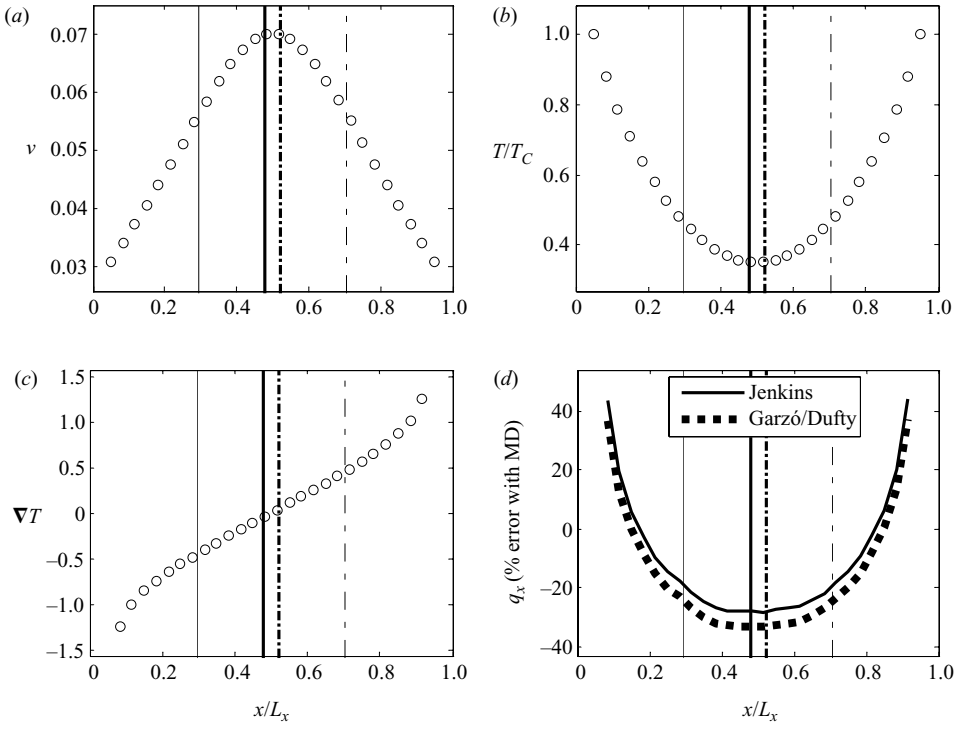

FIGURE 7. MD profiles of (*a*) solids volume fraction, (*b*) non-dimensional granular temperature and (*c*) the first derivative in granular temperature. (*d*) The percentage error in heat flux between MD simulations and theoretical predictions. Symbols and lines are as in figure 2. Relevant parameters are $e = 0.9$, $\bar{\nu} = 0.05$ $(1/Kn = 10.5)$, $T_H/T_C = 1$, $L/d = 35$. Data collection for this simulation involves 200 000 measurements over 10 000 collisions/particle.

in the domain interior is poorer than expected for inelastic systems, with errors of about 30 % for $e = 0.9$. The source of this error is distinct from those caused by the Knudsen layer, and is related to the need to incorporate higher-order effects in the hydrodynamic description. This topic is explored further in Hrenya, Galvin & Wildman (2007), together with analysis of other constitutive quantities, such as those for stress and dissipation rate.

At this point, several comments on the three criteria introduced thus far to identify the thickness of the Knudsen layer are warranted. First, as demonstrated by a comparison of figures 5(*c*) and 5(*d*) at $x/L_x \sim 0.2$, a change in the $\mathrm{d}T/\mathrm{d}x$ profile at the boundary of the Knudsen layer may be subtle, whereas analogous changes in the error associated with q_x predictions are abrupt. Secondly, although errors associated with the other constitutive quantities (stress tensor and dissipation rate of granular energy) were also examined, they do not exhibit as clear a demarcation between the Knudsen layer and bulk interior, and thus are not shown for the sake of brevity (but are contained in Hrenya *et al.* 2007). Thirdly, for systems with non-thermal boundaries, the $(\ell/\lambda)_{wall} = 2.5$ criterion may be less robust than the other two owing to a possible dependence on the detailed nature of the boundaries. Collectively, these observations indicate that the most robust indicator of the Knudsen-layer thickness is that associated with the error in the q_x profiles, and that the $(\ell/\lambda)_{wall} = 2.5$ criterion should be used as a rule-of-thumb (for systems with non-thermal boundaries) if measurements of q_x are unavailable.

As explained in § 3, two different types of comparison between MD simulations and theory are investigated in this work. Up until this point, predictions of the constitutive quantity q_x were obtained using MD profiles of ν and T as inputs to the theoretical expressions, (7) or (8), which was then compared to that extracted directly from MD simulations, (4) and (5). As established above, this comparison is useful in delineating the Knudsen layer. As exemplified below, comparing the ν and T profiles obtained from solution of the BVP to the corresponding MD profiles provides a measure of the appropriateness of Navier–Stokes order theories, coupled with no-slip boundary conditions, for a given thickness of the Knudsen layer. More specifically, figure 8 provides BVP solutions along with MD data for a relatively dense (figure 8*a*, *b*) and dilute (figure 8*c*, *d*) system. The systems are characterized by $T_H/T_C = 1$, $e = 0.99$, and $\bar{\nu} = 0.15$ (dense) and 0.025 (dilute), respectively. As expected, the Knudsen layers are much smaller in the dense system than in the dilute system. For the latter, the lines representing $(\ell/\lambda)_{wall} = 2.5$ almost meet in the middle of the domain (whereas the lines representing $(\ell/\lambda)_{wall} = 5.0$ actually 'cross' one another), indicating that almost the entire domain is made up of the Knudsen layers. As is evident from these plots, the comparison between MD and theoretical predictions is excellent for the dense system in which the combined width of the Knudsen layers take up a relatively small fraction, namely $\sim$20 % combined, of the system domain. For the dilute system, on the other hand, a noticeable mismatch between the MD and theory is observed. This mismatch illustrates the need for slip boundary conditions for inelastic systems. Such conditions, which are well established for rarefied gases (Mackowski *et al.* 1999), represent the value of the hydrodynamic variable extrapolated from the bulk interior to the boundary; i.e. it is an 'apparent' value rather than a 'true' value, with the difference being referred to as the 'slip'. It is worth noting that such corrections to the true value are proportional to the thickness of the Knudsen layer or, equivalently, the mean free path. Thus, as the Knudsen layers become thinner, the apparent value approaches the true value at the boundary. Hence, the BVP solution obtained using true (simulation) values of the wall temperature illustrate the impact of the Knudsen layer, namely systems with relatively small Knudsen layers do not require slip conditions for accurate predictions in the bulk (figure 8*a*, *b*), whereas the opposite is true for systems with larger Knudsen layers (figure 8*c*, *d*).

The above comparison between Navier–Stokes predictions and simulation data provides evidence that such a description, coupled with no-slip conditions, becomes less appropriate as the Knudsen layers begin to dominate this system. This is further

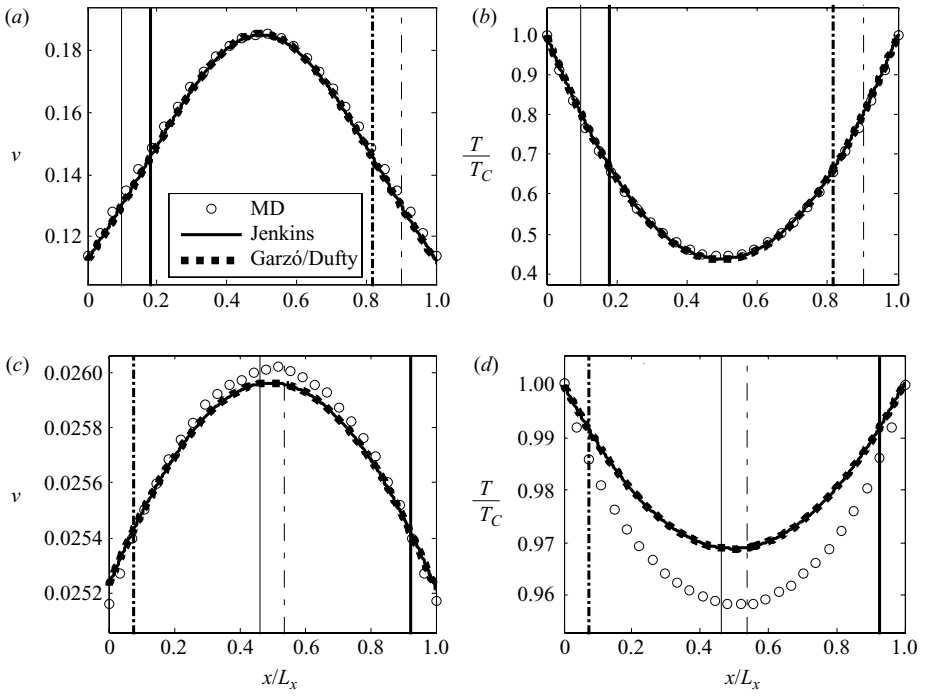

FIGURE 8. Profiles from BVP predictions based on Jenkins (1998) and Garzó & Dufty (1999) theories and from MD simulations of (*a*, *c*) solids volume fraction and (*b*, *d*) non-dimensional granular temperature for two different systems. Symbols and lines are as in figure 2. Relevant parameters for (*a*) and (*b*) are $e = 0.99$, $\bar{\nu} = 0.15$, $T_H/T_C = 1$, $L/d = 35$. Data collection for this simulation involves 200 000 measurements over 10 000 collisions/particle. Relevant parameters for (*c*) and (*d*) are $e = 0.99$, $\bar{\nu} = 0.025$, $T_H/T_C = 1$, $L_x/d = 35$ $(1/Kn = 5.25)$, $L_z/d = L_y/d = 50$. Data collection for this simulation involves 500 000 measurements over 25 000 collisions/particle.

supported by revisiting the experimental data of Viswanathan *et al.* (2006) for a vibro-fluidized bed. Specifically, figure 9 shows granular temperature profiles obtained using positron emission particle tracking (PEPT) for a bed of particles which was vibrated at the base and left open at the top. The radially averaged quantities are shown as a function of vertical distance, in which the positive z-direction is opposite to the direction of gravity (g). Temperature measurements associated with two directions are shown separately, namely $T_r = C_r^2$ and $T_z = C_z^2$, along with their scalar counterpart $T = (T_r + T_x + T_z)/3$; the other horizontal component T_x is not shown since it is similar to T_r, which is the more accurate of the two horizontal measurements. Experiments were conducted for relatively dense (low vibrational amplitude) (figure 9*a*) and dilute (high vibrational amplitude) (figure 9*b*) systems. Specifically, results for dimensionless base velocities of $V^* = V/\sqrt{gd} = 0.74$ and 1.54 (figures 9*a* and 9*b*, respectively) are displayed, where V is the velocity of the vibrating base. A vertical line is again shown in the plots for $(\ell/\lambda)_{wall} = 2.5$ to estimate the Knudsen layer originating from the vibrating base; this line is determined based on the experimental measurements of solids fraction as reported Viswanathan *et al.* (2006). (A similar line denoting the Knudsen layer at the open end of the system is not included since the bed height in an open container is not well-defined; estimates for the Knudsen-layer thickness at such an open boundary can be found in Pasini & Jenkins 2005.) Also plotted are

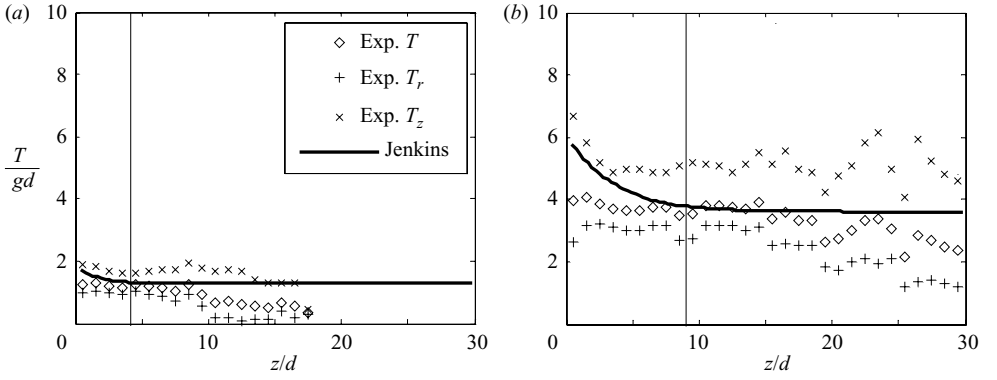

FIGURE 9. Temperature profiles in vibro-fluidized bed from BVP predictions of Viswanathan *et al.* (2006) based on Jenkins (1998) theory (solid line) and from experimental PEPT data (individual symbols) of Martin *et al.* (2006). Reciprocal local Knudsen number of 2.5 evaluated from the vibrating bottom boundary is indicated by a vertical solid line. Relevant parameters are (*a*) $V^* = 0.74$ (dense) and (*b*) $V^* = 1.54$ (dilute).

the corresponding theoretical temperature (T) predictions of Jenkins (1998) obtained from the solution of a two-dimensional boundary-value problem. The BVP associated with this system differs from that of the MD system examined earlier owing to the increased dimensionality, the presence of a gravitational field, and the use of no-slip boundary conditions (details are available in Viswanathan *et al.* 2006). Similar to the experimental measurements, the two-dimensional profiles are averaged in the radial direction and thus plotted as a function of z only. For the denser system (figure 9*a*), the Knudsen layer takes up roughly 20 % of the domain and the model predictions for T and corresponding PEPT data are seen to be in fairly good agreement throughout the domain. For the more dilute system (figure 9*b*), a noticeable mismatch between model predictions and experimental data occurs in the Knudsen layer, which represents about 30 % of the domain. As a further testament to the presence of Knudsen-layer effects in the dilute system, the experimental data of figure 9(*b*) clearly indicate that the axial component of the temperature (T_z) 'jumps' to a higher value at the base, which is characteristic of the temperature profile in the Knudsen layer near a hot wall, or energy source (Mackowski *et al.* 1999). A similar jump is not observed in the denser system (figure 9*a*) owing to the reduced size of the layer. Note that a temperature jump in the direction perpendicular to the vibrating plate (T_r) is not observed in either case since the vertically vibrated bed provides an (anisotropic) energy source primarily in the vertical direction. Hence, the model–data mismatch noted above for the dilute system may arise from either the lack of an 'apparent slip' boundary condition targeted at systems with non-negligible Knudsen layers (Mackowski *et al.* 1999) and/or the use of an isotropic theory in an anisotropic region. However, because particle–particle collisions will reduce the level of anisotropy caused by the vibrating base, the observed anisotropy is also restricted to the Knudsen-layer region (where particle–particle collisions play only a small role), and hence both potential causes of mismatch are tied to the presence of a non-negligible Knudsen layer.

5. Concluding remarks

The thrust of this effort has been twofold: (i) to identify the Knudsen layer in granular flows; and (ii) to assess its impact on predictions obtained from a Navier–Stokes

order theory applied across the domain with standard (no-slip) boundary conditions. First, it has been shown that the standard approaches used for identification of the Knudsen layer in molecular gases are not as useful for granular systems, since the presence of dissipation (i) may mask the abrupt change in the $\mathrm{d}T/\mathrm{d}x$ profile, and (ii) precludes the use of the criterion based on the violation of Fourier's law (as heat flux is no longer constant). These shortcomings are overcome via an examination of the percentage error between MD data and Navier–Stokes order predictions for the heat flux (in which MD profiles of ν and T are used to evaluate the theoretical expression). When this comparison is performed, a substantial increase in the mismatch between simulation and theory is observed, which provides a clearcut demarcation between the Knudsen layer and the bulk interior for both elastic and inelastic systems. For systems in which heat flux measurements are not readily available (such as experimental systems), $\ell_{bl} = 2.5\lambda_{wall}$ provides a rule-of-thumb for Knudsen-layer thickness; this quantity (for a molecular gas in thermal equilibrium) corresponds to a distance from the wall in which fewer than 10 % of the particles travelling that distance have not undergone a collision with another particle.

Secondly, the impact of the Knudsen layer on ν and T predictions obtained from Navier–Stokes theory with standard (no-slip) boundary conditions has been examined via a comparison with both MD simulations and previous experimental data (Viswanathan *et al.* 2006) The comparison is quite good when the combined Knudsen layers represent about 20 % of the system domain, whereas deterioration of the theory is evident when the domain is made up entirely of the Knudsen layer. The level of mismatch for the latter case, however, is perhaps less than might be expected, suggesting that the domain of validity for Navier–Stokes theory is greater than that afforded by a strict interpretation of the separation-of-scale assumptions. Although outside of the scope of the current effort, it is anticipated that the domain of validity could be further increased via the use of apparent (or slip) boundary conditions as is the standard approach for molecular gases with increasing rarefication.

In addition to the impact of the Knudsen layer on theoretical predictions, its impact on MD analysis and experimental design is also noteworthy. First, in several previous works, the heat flux has been extracted directly from MD simulations, either for development of a correlation (Soto, Mareschal & Risso 1999) or for comparison with theory (Shattuck *et al.* 1999; Herbst *et al.* 2005). As is illustrated in the current work, care should be taken to ensure that such heat flux data are not extracted in the Knudsen layer, as the heat flux in the Knudsen layer takes on different values from that in the bulk region. Analogous cautions are also recommended for other constitutive quantities, namely stress and dissipation rate. Alternatively, when using MD simulations to study the bulk interior, boundary conditions which effectively eliminate the presence of the Knudsen layer may be helpful, as have been used previously in direct simulation Monte Carlo studies of elastic systems (e.g. Montanero *et al.* 1994; Mackowski *et al.* 1999). Secondly, for experiments designed as tests of Navier–Stokes order theory, the size of the Knudsen-layer should be kept in check.

It is also worth noting that much recent interest has been focused on the form of the heat flux law for granular materials, and particularly on the importance of the term proportional to the concentration gradient (Sela & Goldhirsch 1998; Soto *et al.* 1999; Herbst *et al.* 2005; Martin *et al.* 2006). For the bounded conduction problem examined in this work, this term does not play an important role, as is evidenced by the consistent agreement between the theories of Jenkins (1998) and Garzó & Dufty (1999), the former of which contains only a term proportional to the temperature gradient, and the latter of which contains both terms.

Finally, although the focus of the current effort has been on the Knudsen layer, an unexpected level of mismatch between the theoretical predictions for the heat flux and the corresponding MD values is observed in the domain interior (bulk region). This behaviour, as well as that of the other constitutive quantities (stress and dissipation rate) in the domain interior, are further explored in Hrenya *et al.* (2007).

The authors would like to express their gratitude to Harish Viswanathan for providing model predictions for the vibrating bed system. Funding for this work has been provided by the Engineering and Physical Sciences Research Council (Grants EP/D030676/1 and GR/R75694/01). J. E. G. and C. M. H. would also like to thank the National Science Foundation for partial funding support via an international supplement to Grant CTS-0318999. C. M. H. and R. D. W. are also grateful to the organizers and participants of the Granular Physics Workshop at the Kavli Institute of Theoretical Physics (supported in part by the National Science Foundation under Grant PHY99-07949), as numerous discussions at the workshop provided the motivation for much of this work.

REFERENCES

Arnarson, B. O. & Jenkins, J. T. 2004 Binary mixtures of inelastic spheres: simplified constitutive theory. *Phys. Fluids* **16**, 4543.

Behringer, R. P., van Doorn, E., Hartley, R. R. & Pak, H. K. 2002 Making a rough place 'plane': why heaping of vertically shaken sand must stop at low pressure. *Gran. Matter* **4**, 9.

Bird, G. A. 1994 *Molecular Gas Dynamics and the Direct Simulation of Gas Flows*. Clarendon.

Brey, J. J., Ruiz-Montero, M. J. & Moreno, F. 2001 Hydrodynamics of an open vibrated system. *Phys. Rev.* E **63**, 061305.

Carnahan, N. F. & Starling, K. E. 1969 Equation of state of non-attracting rigid spheres. *J. Chem. Phys.* **51**, 635.

Cercignani, C. 1987 *The Boltzmann Equation and its Applications*. Springer.

Cercignani, C., Illner, R. & Pulvirenti, M. 1994 *The Mathematical Theory of Dilute Gases*. Springer.

Chapman, S. & Cowling, T. G. 1970 *The Mathematical Theory of Non-Uniform Gases*. Cambridge University Press.

Ciccotti, G. & Tenebaum, A. 1980 Canonical ensemble and nonequilibrium states by molecular dynamics. *J. Stat. Phys.* **23**, 767.

Clause, P. J. & Mareschal, M. 1988 Heat-transfer in a gas between parallel plates – moment method and molecular-dynamics. *Phys. Rev.* A **38**, 4241.

Dahl, S. R. & Hrenya, C. M. 2004 Size segregation in rapid, granular flows with continuous size distributions. *Phys. Fluids* **16**, 1.

Ferziger, J. H. & Kaper, H. G. 1972 *Mathematical Theory of Transport Processes in Gases*. Elsevier.

Forterre, Y. & Pouliquen, O. 2001 Longitudinal vortices in granular flows. *Phys. Rev. Lett.* **86**, 5886.

Galvin, J. E., Dahl, S. R. & Hrenya, C. M. 2005 On the role of non-equipartition in the dynamics of rapidly flowing granular mixtures. *J. Fluid Mech.* **528**, 207.

Garzó, V. & Dufty, J. 1999 Dense fluid transport for inelastic hard spheres. *Phys. Rev.* E **59**, 5895.

Goldhirsch, I. 2003 Rapid granular flows. *Annu. Rev. Fluid Mech.* **35**, 267.

Goldhirsch, I., Noskowicz, S. H. & Bar-Lev, O. 2004 Theory of granular gases: some recent results and some open problems. *J. Phys.: Condens. Matter* **17**, 2591.

Herbst, O., Müller, P. & Zippelius, A. 2005 Local heat flux and energy loss in a two-dimensional vibrated granular gas. *Phys. Rev.* E **72**, 141303.

Hopkins, M. & Louge, M. 1991 Inelastic microstructure in rapid granular flows of smooth disks. *Phys. Fluids* A **3**, 47.

Hrenya, C. M., Galvin, J. E. & Wildman, R. D. 2007 Evidence of higher-order effects in thermally-driven, granular flows. *J. Fluid Mech.* (Submitted).

Jenkins, J. T. 1998 Kinetic theory for nearly elastic spheres. In *Physics of Dry Granular Media* (ed. H. J. Hermann, J. P. Hovi & S. Luding). Kluwer.

Jin, S. & Slemrod, M. 2001 Regularization of the Burnett equations for rapid granular flows via relaxation. *Physica* D **150**, 207.

Kadanoff, L. P. 1999 Built upon sand: theoretical ideas inspired by granular flows. *Rev. Mod. Phys.* **71**, 435.

Kierzenka, J. & Shampine, L. F. 2001 A BVP solver based on residual control and the Matlab pse. *ACM Trans. Math. Software* **27**, 299.

Kumaran, V. 1997 Velocity distribution function for a dilute granular material in shear flow. *J. Fluid Mech.* **340**, 319.

Kumaran, V. 2005 Kinetic model for sheared granular flows in the high Knudsen number limit. *Phys. Rev. Lett.* **95**, 108001.

Mackowski, D., Papadopoulos, D. H. & Rosner, D. E. 1999 Comparison of Burnett and DSMC predictions of pressure distributions and normal stress in one-dimensional, strongly nonisothermal gases. *Phys. Fluids* **11**, 2108.

Mareschal, M., Kestemont, E., Baras, F., Clementi, E. & Nicolis, G. 1987 Nonequilibrium states by molecular-dynamics – transport-coefficients in constrained fluids. *Phys. Rev.* A **35**, 3883.

Martin, T. W., Huntley, J. M. & Wildman, R. D. 2006 Hydrodynamic model for a vibrofluidized granular bed. *J. Fluid Mech.* **535**, 325.

Montanero, J. M., Alaoui, M., Santos, A. & Garzó, V. 1994 Monte Carlo simulation of the Boltzmann equation for steady Fourier flow. *Phys. Rev.* E **49**, 367.

Pan, L. S., Xu, D., Lou, J. & Yao, Q. 2006 A generalized heat conduction model in rarefied gas. *Europhys. Lett.* **73**, 846.

Pasini, J. M. & Jenkins, J. T. 2005 Aeolian transport with collisional suspension. *Phil. Trans. Royal Soc.* A – *Math. Phys. Engng Sci.* **363**, 1625.

Pöschel, T. & Schwager, T. 2005 *Computational Granular Dynamics*. Springer.

Press, W. H., Flannery, B. P., Teukolsky, S. A. & Vetterling, W. T. 1992 *Numerical Recipes in C: The Art of Scientific Computing*. Cambridge University Press.

Rericha, E. C., Bizon, C., Shattuck, M. D. & Swinney, H. L. 2002 Shocks in supersonic sand. *Phys. Rev. Lett.* **88**, 014302.

Rosner, D. E. & Papadopoulos, D. H. 1996 Jump, slip and creep boundary conditions at nonequilibrium gas/solid interfaces. *Ind. Engng Chem. Res.* **35**, 3210.

Santos, A. & Garzó, V. 1995 In *Rarefied Gas Dynamics 19* (ed. J. Harvey & G. Lord). Oxford University Press.

Sela, N. & Goldhirsch, I. 1998 Hydrodynamic equations for rapid flows of smooth inelastic spheres, to Burnett order. *J. Fluid Mech.* **361**, 41.

Shattuck, M. D., Bizon, C., Swift, J. B. & Swinney, H. L. 1999 Computational test of kinetic theory of granular media. *Physica* A **274**, 158.

Sone, Y. 2002 *Kinetic Theory and Fluid Dynamics*. Birkhause.

Soto, R., Mareschal, M. & Risso, D. 1999 Departure from Fourier's law for fluidized granular media. *Phys. Rev. Lett.* **83**, 5003.

Viswanathan, H., Wildman, R. D., Huntley, J. M. & Martin, T. W. 2006 Comparison of kinetic theory predictions with experimental results for a vibrated three-dimensional granular bed. *Phys. Fluids* **18**, 113302.

Wassgren, C. R., Cordova, J. A., Zenit, R. & Karion, A. 2003 Dilute granular flow around an immersed cylinder. *Phys. Fluids* **15**, 3318.

Wildman, R. D., Jenkins, J. T., Krouskop, P. E. & Talbot, J. 2006 A comparison of the predictions of a simple kinetic theory with experimental and numerical results for a vibrated granular bed consisting of nearly elastic particles of two sizes. *Phys. Fluids* **18**, 073301.